Collisional ionization and excitation of H₂: Two-electron processes

A. K. Edwards, R. M. Wood, and J. L. Davis

Department of Physics and Astronomy, University of Georgia, Athens, Georgia 30602

R. L. Ezell

Department of Chemistry and Physics, Augusta College, Augusta, Georgia 30910

(Received 24 January 1990)

The cross sections for the double ionization, ionization plus excitation, and double excitation of H₂ by electrons and protons in the range of 350 to 3500 keV/amu have been measured. In all cases, the cross section for electron bombardment was greater than that for equivelocity proton bombardment. The results are discussed in terms of first and second Born processes and interferences between the two.

I. INTRODUCTION

When a fast projectile interacts with a two-electron system, such as helium or H₂, several events can occur that involve both electrons. These include double ionization, ionization plus excitation, and double excitation. Also, several different interactions can produce these events. They are illustrated in the Goldstone diagrams shown in Fig. 1 and are the following: (a) The projectile interacts separately with each electron in a double-collision process producing the final state. No electron correlation is involved. (b) The electrons are excited to virtual states through ground-state correlation and then excited to the final state by the single projectile-electron interaction. (c) The projectile interacts with one electron imparting energy to it, and it in turn interacts with the other electron leading to ionization or excitation. (d) The projectile removes or excites one electron from the ground state producing a hole, and the other electron is removed by the projectile and the remaining ion relaxes to an excited or continuum state. With the exception of the double-collision process, all of these interactions have been considered by Carter and Kelly[1] in the double photoionization of helium. Unlike the photoionization case, however, the Coulomb interaction of the projectile allows nondipole as well as dipole excitations. The terminology evolving from recent work[2] is to refer to the double-collision process as two-step 2 (TS-2), the projectile-electron collision followed by an electron-electron interaction as two-step 1 (TS-1), and the electron-hole interaction as shake-off or shake-up, meaning, respectively, that the second electron is removed or excited.

Helium has been the most thoroughly studied target, both experimentally[2-11] and theoretically.[1,12-20] H₂ has been shown experimentally[21] to have many of the same characteristics of helium with regard to the two-electron events described above. Most of the work[21,22] has concentrated on double ionization by positive and negative projectiles. It has been clearly demonstrated[4] that negative projectiles, whether they are antiprotons or electrons, have about twice the cross section for double ionization as do equivelocity positive projectiles, whether

they are protons or positrons. Several different theoretical models have been proposed in order to explain this difference.[12-20]

McGuire[13,14] suggested that the factor-of-2 difference in double ionization was due to an interference effect between the double-collision process (TS-2) and shakeoff. Reading and Ford[12] placed the idea of an interference effect on a more solid footing. They developed a forced-impulse method (FIM) to calculate the double-ionization cross section and expressed their results in a Born series in the projectile charge Z_p,

$$\sigma^{2+} = a(v_p)Z_p^2 - b(v_p)Z_p^3 + c(v_p)Z_p^4 , \qquad (1)$$

where v_p is the projectile velocity. The Z_p^3 term is due to

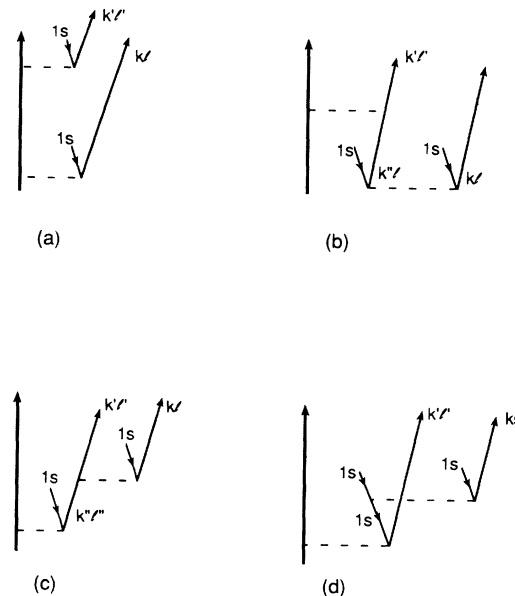(a)   (b)

(c)   (d)

FIG. 1. Goldstone diagrams for the two-electron process included in ionization and excitation of helium by a fast projectile. (a) Double collision without correlation. (b) Ground-state correlation plus collision. (c) Collision plus electron-electron interaction. (d) Collision plus electron-hole interaction. The final state kl can be either continuum or bound state.
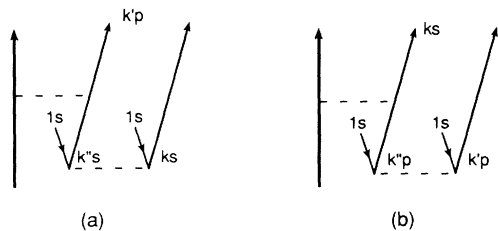
FIG. 2. Goldstone diagrams for excitation to $ksk'p$ $^1P^o$ by ground-state correlation to (a) $k''sks$ $^1S^e$ or (b) $k''pk'p$ $^1S^e$ virtual state and a dipole interaction.

FIG. 3. Schematic of the experimental apparatus. Only analyzer A is used in the present work. Both analyzers have been used in coincidence measurements mentioned in the text.

an interference between the first and second Born terms; it is a negative quantity which means that it enhances σ^{2+} for negative projectiles and reduces it for positive projectiles. Reading and Ford went on to show that it is a nondipole contribution to the projectile-electron interaction that is responsible for the interference term.

The double-collision process shown in Fig. 1(a) is a second Born process in the projectile-electron interaction whereas those in Figs. 1(b)–1(d) are first Born. For a given final-state configuration the diagrams can be used to determine whether or not the collision is dipole or nondipole in nature and which of the subsequent processes are allowed. For example, if the final state is $ksk'p$ $^1P^o$ and ground-state correlation is the interaction of interest then Figs. 2(a) and 2(b) show that the projectile interaction is dipole. For the second Born contribution of Fig. 1(a) there must be a nondipole interaction to produce the ks electron. But, if the final state is $kpk'p$ $^1S^e$, $^1P^e$, or $^1D^e$ then the first Born projectile interaction is nondipole and the second Born contribution is two dipole interactions.

When H_2 is the system studied, all of the two-electron events listed above, namely, double ionization, ionization plus excitation, or double excitation, lead to dissociative states of the H_2 ion.[23,24] The kinetic energy released when the ion dissociates is a signature of the potential curve of the ionic state. By measuring the kinetic energy of the fragment H^+ ion that is produced in dissociation, one can determine the excited states formed in the collisions of fast projectiles with H_2. This makes it possible to measure the cross section for excitation of both dipole and nondipole allowed states. In what follows, only σ_g, σ_u, and π_u orbitals of H_2 are considered and the projectile-electron interaction is considered to be primarily, but not totally, a dipole one. The ground state of H_2 is a σ_g^2 configuration which means that the nondipole contributions from the projectile-electron interaction would result in a σ_g to σ_g transition and the dipole contributions would be a σ_g to σ_u or π_u transition. In the diagrams of Fig. 1, the helium s states become σ_g states of H_2 and the p states become either σ_u or π_u.[25]

II. EXPERIMENTAL PROCEDURES

The cross sections for the different pathways for ionization and dissociation of the H_2 target molecules were measured using a time-energy-spectroscopy (TES) technique described in earlier work from our laborato-
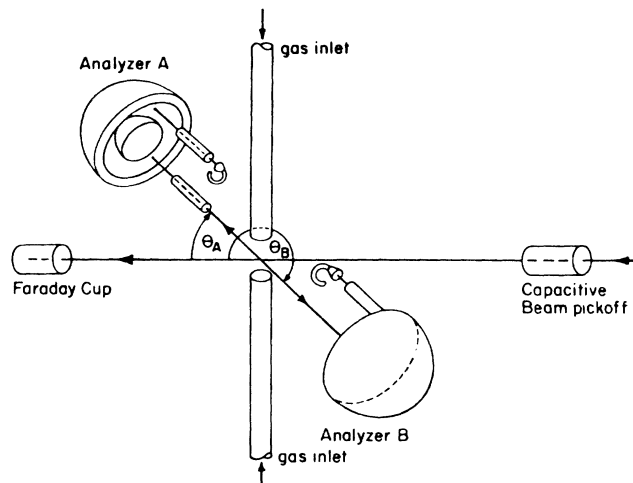
ry.[21,26,27] A pulsed beam of electrons or protons was passed through a differentially pumped collision region and collected in a biased Faraday cup as illustrated in Fig. 3. By methods to be described later, the target gas pressure in the interaction region was measured to be 1.3×10^{-4} Torr. The pressure in the surrounding vacuum vessel was approximately 5×10^{-6} Torr.

In the present work a single hemispherical analyzer and its associated focusing elements were positioned in the horizontal plane at an angle of 90° with respect to the projectile beam direction. The solid angle subtended by the analyzer was 3.05×10^{-3} sr. The section of the projectile beam which could be viewed by the analyzer was 0.178 cm long. The H^+ ions emitted in the dissociation processes drifted through a 4.45-cm field-free region and were then focused by an accelerating lens onto the entrance slit of the analyzer. The analyzer voltages were adjusted to pass ions with ten times the energies E_0 with which they were emitted in the initial dissociation events. The energy resolution of the analyzer was $\Delta E = 0.15 E_0$ [full width at half-maximum (FWHM)]. After exiting the analyzer, the ions were further accelerated by a 2300-V potential difference and fell incident on a channel electron multiplier.

The TES technique requires the simultaneous measurement of the time of flight (TOF) and kinetic energy of an ionic fragment emitted in the dissociative ionization of a molecule. Measuring both TOF and energy permits the fragments of differing mass-to-change ratio to be identified and analyzed separately. In this work, the H^+ ions of interest were clearly separated from contaminant ions such as N^+, N^{2+}, and O^+ which arose from projectile collisions with background gases. Measurements made with the target gas removed showed a negligible number of background H^+ ions were present.

Two pieces of information are provided about each detected ion: its energy and its TOF. The data are recorded in a two-parameter array in a multichannel analyzer. The x coordinate of a particular recorded event

is proportional to the fragment's energy; the y coordinate is proportional to the fragment's TOF. Ions with a specific m/q ratio are consequently represented by a unique curve in the two-parameter data array.

The TOF of the detected ion is measured using standard pulsed beam TOF methods. The proton beam was taken from a Van de Graaff accelerator and consisted of pulses which were approximately 150 ns in duration separated by 32 μs. The electron beam was obtained from an electron gun which delivered pulses approximately 1 μs wide separated by 64 μs. Since one of the objectives of this work was to compare electron- and proton-induced cross sections, care was taken to insure that the proton and electron beams followed exactly the same path and exhibited the same spatial profile.[21]

In order to record H^+ ions with energies in the range from 1 to 15 eV, the voltages applied to the analyzer and focusing elements were derived from a low-frequency triangular waveform generator. The energy scale of the analyzer was calibrated by observing ionizing processes which produce ions with known kinetic-energy peaks.

In Sec. III of this paper it is explained that the peak in the kinetic-energy distribution of H^+ ions coming from the double ionization of H_2 falls at 9.36 eV. Using coincidence techniques described earlier,[21,22,28] the point on the energy scale of the analyzer corresponding to 9.36 eV was determined. Other calibration points were also used: a group of 2.0-eV O^+ ions from the dissociative ionization of O_2,[29,30] a group of 3.9-eV N^+ ions from the dissociation of N_2,[31] a group of 4.31-eV H_3^+ ions from the dissociation of C_2H_6,[32] and the 0-eV point obtained by extrapolation of the voltages applied to the analyzer. All of the above-mentioned points were determined and a least squares fit was performed giving greatest weight to the 9.36 and 2.0-eV points which are the best known.

In order to measure absolute cross sections for the various ionization channels, the number of target molecules in the interaction region must be accurately determined. To do this the known cross section for the Rutherford scattering of 1-MeV protons by argon was used to calculate the target gas pressure. Analyzer B in Fig. 3 was replaced by a surface barrier detector, but the defining apertures, which determine the solid angle and other geometrical parameters, were not changed. The yields at scattering angles of 42°, 36°, 30°, 24°, and 18° were measured and the effective argon target thickness was calculated at each angle. The results of the measurements showed that the target gas density is uniform to better than 1% over the interaction region viewed by the detector down to an observation angle of 30°, and therefore is uniform over the 0.178-cm-long interaction region viewable at 90°.

Target gas pressure was set with a needle valve and monitored by a capacitance manometer. In order to establish that the pressure in the interaction region corresponding to a given manometer reading was the same for the argon used in the Rutherford scattering measurements and the H_2 gas used in the dissociative ionization measurements, a computer code was used.[33] The code calculates gas density at the end of a tube connected to a gas reservoir. The calculations indicated that there was less than a 2% difference between H_2 and Ar target densities for the same reservoir pressure under the conditions of our experiment.

The uncertainty in the absolute value of the target gas density as measured by the Rutherford scattering technique was due mostly to an uncertainty in the scattering angle. The maximum angular divergence of the proton beam was 7×10^{-3} rad and the detector could be placed to an accuracy of 10×10^{-3} rad. The capacitance manometer was monitored in order to keep the target gas pressure variations less than 1%. The statistical error of the counts of the scattered protons was less than 2%. The net effect was an uncertainty of 12% in the target gas density.

III. DATA REDUCTION

The first step in analyzing the two-parameter TOF energy array is to determine the yield of H^+ ions as a func-
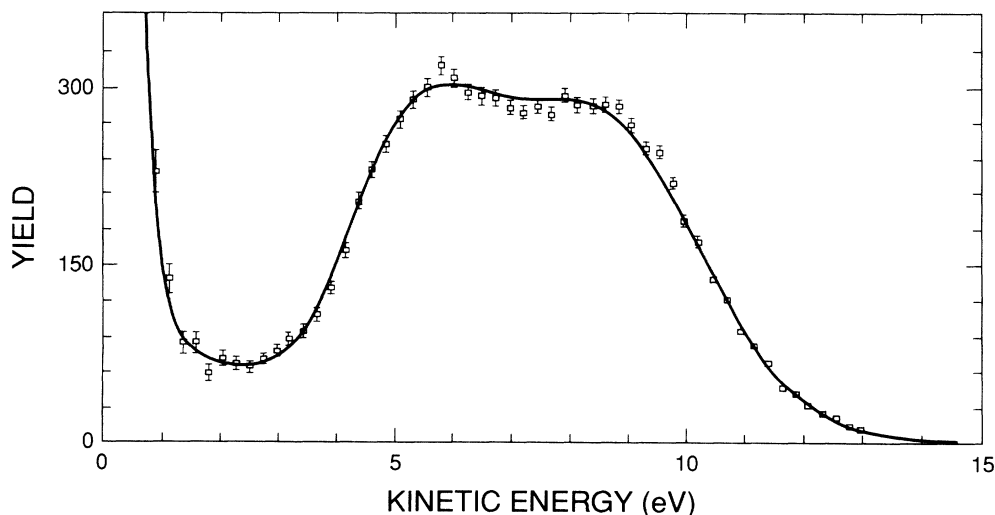

FIG. 4. H^+ ions from the dissociative ionization of H_2 by 0.5-MeV/amu protons.

tion of ion kinetic energy. An energy-dependent correction must be applied to the yield because the triangular energy-resolution function of the analyzer causes the fraction of ions passed by the analyzer to increase linearly with ion energy. The result of the correction is the kinetic energy spectrum of the H^+ ions from all the possible dissociative ionization processes. A typical example of a corrected energy distribution is shown in Fig. 4.

The spectrum is a smoothly varying overlap of the ions produced in the several dissociation channels under consideration. In order to determine how much each channel contributes to the total yield, one needs to calculate a predicted kinetic-energy distribution for each channel. In earlier work[27,34] reported from this laboratory, the kinetic energy spectra were predicted using the reflection approximation. In the case of the autoionizing states no prediction could be made because potential curves were not available.

In the present work the predicted kinetic-energy distributions for the ionization plus excitation and the double-ionization channels were computed by Heil.[35] In his calculation the overlap of the ground-state and the excited-state wave functions was calculated by direct numerical integration of the Schrödinger equation. The ground-state wave function was found by the method of Zare and Cashion.[36] The population of rotational states in the H_2 ground state was taken into account by inclusion of $J = 0$–4 states with appropriate weights.

The potential curves for the $1s\sigma_g$, $2p\sigma_u$, $2p\pi_u$, and $2s\sigma_g$ were those of Sharp.[24] The outgoing wave for the dissociative state was found by a Numerov procedure and was energy normalized.[37] The overlap was calculated for a large number of internuclear separations of the nuclei in the H_2 molecule. Vertical transitions were assumed. In each case, the resulting spectrum was broadened with a Maxwell-Boltzmann distribution to allow for the translational thermal motion of the molecules in the H_2 target.[38] The kinetic-energy distribution for the double-ionization channel was computed in the same way, but the repulsive curve is simply the pure Coulomb potential

for two protons. Figure 5 shows the results of the calculations. The figure is presented because the new calculations differ slightly from the older reflection approximation results cited earlier.[27]

In order to fit the measured kinetic-energy distribution of all H^+ ions shown in Fig. 4 with the predicted kinetic-energy distributions for each dissociation channel, the energy resolution of the analyzer used in the experiment must be considered. This was a small effect but was taken into account by broadening the distributions of Fig. 5 with the transmission function of the hemispherical analyzer.

When the fitting functions shown in Fig. 5 are compared to the data in Fig. 4, it can be observed that there is yield in the 3-eV region which cannot be accounted for by ionization plus excitation or double ionization. We suggest that this yield is due to autoionizing processes involving the excitation of both electrons in the H_2 molecule. Three doubly excited states of H_2 were considered: $^1\Pi_g$, $^1\Sigma_g^+$, and $^1\Sigma_u^+$. Potential curves for these states have been published by Guberman.[39] The curves lie close together just below the curve for the $2p\sigma_u$ of H_2^+, and cross the $1s\sigma_g$ curve at internuclear separations in the 2–4 bohr range. The autoionization takes place when there is a transition from the doubly excited state of H_2 to the $1s\sigma_g$ ground state of H_2^+.

We used the reflection approximation to calculate the predicted kinetic-energy spectrum for each of the autoionizing states. An important parameter in that calculation is the lifetime of each of the states. The lifetimes are dependent on the internuclear separation R, and were computed using the energy width calculated by Tennyson and Noble.[40]

A rough outline of the calculation is as follows. A first value for the internuclear separation of the H_2 ground state is chosen. A vertical transition to the autoionizing state is allowed. The nuclei separate along the potential curve for a short-time interval. The probability of decay in that interval is calculated. The kinetic energy of the H^+ ion is calculated assuming decay at the end of the time interval. The contribution of H^+ ions with this kinetic energy is weighted by the probability of decay. The nuclei are permitted to separate further for another time increment and the calculations of decay probability and kinetic energy are repeated. This process is continued until the internuclear separation exceeds that corresponding to the point where the autoionizing curve crosses the $1s\sigma_g$ curve of H_2^+. At this point, the whole process is repeated with another value for the initial separation of the nuclei in the H_2 molecule. When all appropriate internuclear separations have been chosen and appropriately weighted by the amplitude of the ground-state wave function, the calculation is complete.

The results of the calculations for the states considered are shown in Fig. 6. As can be seen, the predicted distributions are broad and contribute H^+ ions mostly in the 0–5 eV range. Our experimental method does not permit us to distinguish between contributions from the three states. In order to proceed, an essentially arbitrary mix of the curves was chosen as the fitting function which would represent all autoionizing processes. The chosen
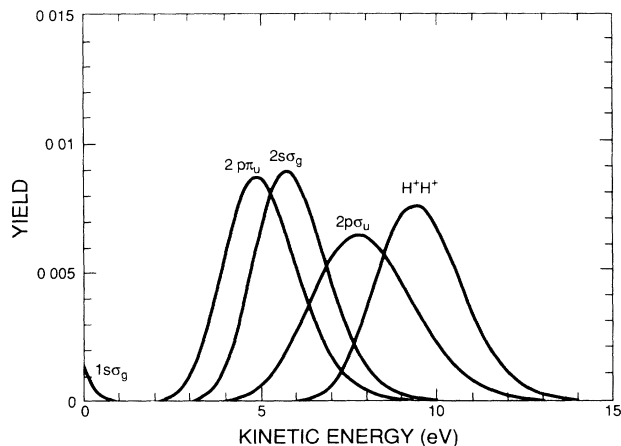
FIG. 5. Predicted kinetic-energy distributions of H^+ ions from the states indicated. The spectra have been broadened for thermal motion.
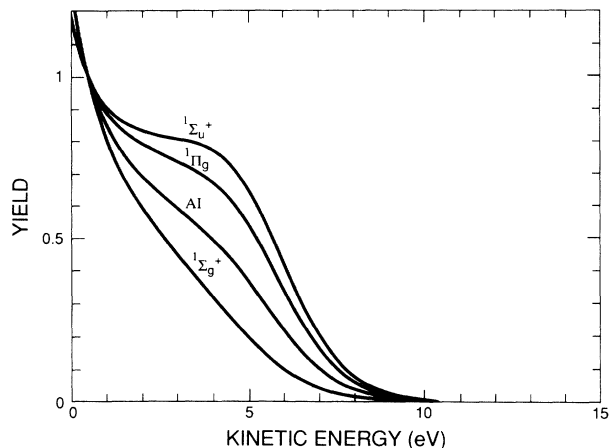
FIG. 6. Predicted kinetic-energy distributions of H^+ ions from doubly excited states of H_2. The spectrum labeled AI is used in the fit.

mix, yielded the best fit, was equal parts of the $^1\Pi_g$ and $^1\Sigma_g^+$ distributions and is labeled AI (for autoionization) in Fig. 6.

In summary, there were six fitting functions. Five are shown in Fig. 5, and the sixth is the curve labeled AI shown in Fig. 6. These six functions were used to fit the measured kinetic-energy distributions such as the one in Fig. 4. A grid search procedure was followed in which only the amplitudes of the six fitting functions were allowed to vary in such a way as to minimize chi square. Since our measurements are uncertain at very low kinetic energies, only the data between 0.85 and 13.2 eV were utilized in the fitting process.

The fit to the data in Fig. 4 is shown in Fig. 7. The amount of each fitting function needed to achieve the fit is also shown. By integrating each of the fitting functions, the H^+ yield contributed by each ionization channel could be determined. The yields were reduced to cross sections in the usual way.

The statistical uncertainty in the contribution of each

state as determined by the fitting procedure was typically less than 3%. A larger variation occurred for a small change in the calibration of the energy axis. This variation was estimated to give an uncertainty in the fitting results of about 5%. Combining these uncertainties with those of the target gas density mentioned above yields a net uncertainty of about 15% in the cross sections.

Inclusion of $n = 3$ excited states of H_2^+ in the calculations was considered but rejected. The predicted kinetic-energy distributions for the $n = 3$ states peak at about 6 eV, and when included in the grid search fitting procedure, the fit to the data did not improve. Furthermore, the electronic overlap between the H_2 ground state and one of the $n = 3$ states of H_2^+ is expected to be smaller than the same overlap with the $n = 2$ states.

In the case of the double-ionization channel, the results of the present work can be compared to earlier measurements made with a different experimental procedure. In the earlier work,[21] we reported on the coincident measurement of both H^+ fragments released in the double-ionization process. The experiment involved the placement of two analyzers on opposite sides of the interaction region to accept the H^+ ions as they separated from one another along a straight line path. In the coincidence measurements it was difficult to determine geometrical effects associated with the analyzers and target accurately, so that the uncertainty in the absolute cross sections was large. The new method used in the present work yields more accurate values of absolute cross sections. The relative values of the cross sections for double ionization as evidenced by the energy dependence of the yields is the same in the two experiments to well within experimental uncertainties.

IV. RESULTS

A. Double ionization

The cross sections for double ionization of H_2 by electrons and protons are shown in Fig. 8 and listed in Table
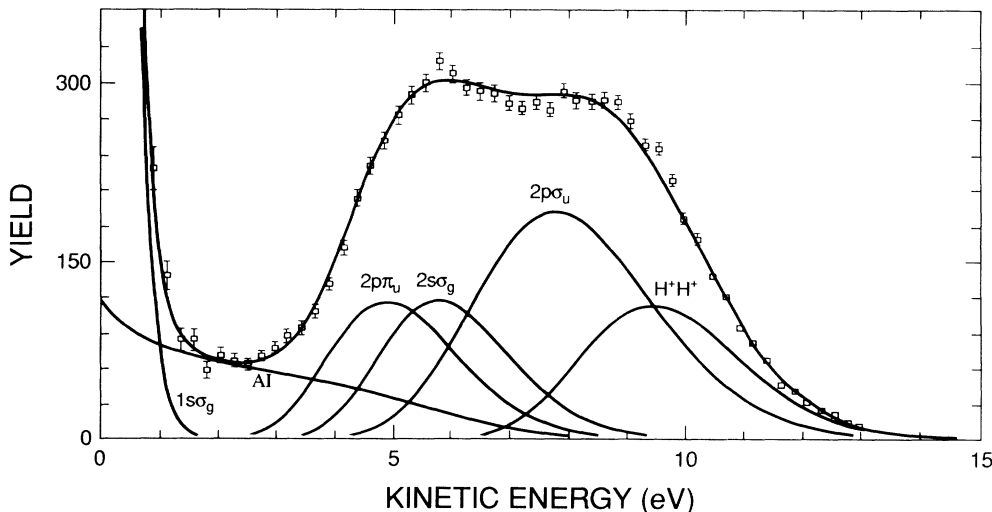

FIG. 7. The smooth line through the data is the result of a least-square fit. The contribution of each state is shown.
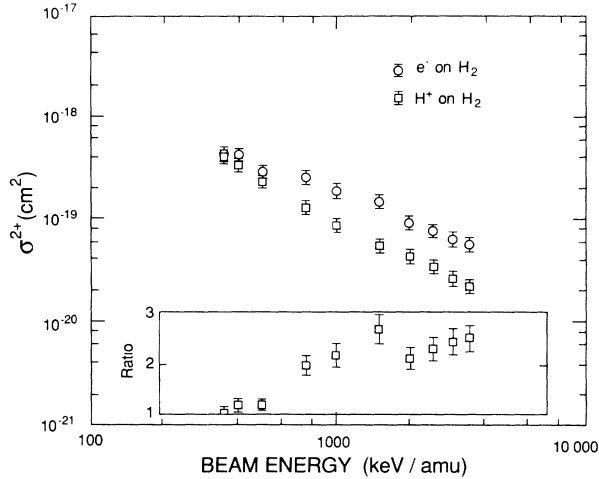
FIG. 8. Cross sections for double ionization of H_2 by electrons and protons. Ratios of cross sections by electrons to protons are shown in the enclosed box.

I. These are corrected values of the results published earlier.[21] The electron results are, on the average, 33% higher than those reported by Schmidt and co-workers.[41] The falloff of the electron data at low beam velocities is due to the high threshold energy for double ionization. At 750 keV/amu and above, the ratios of double-ionization cross sections for electron to proton bombardment is about 2.3 and is fairly constant. It is assumed here that this occurs in H_2 for the same reason as it does in helium,[12] i.e., it is an interference between first and second Born processes, and the main contribution to the interference occurs because of a nondipole transition produced by the projectile-electron interaction. With Z_p in Eq. (1) being -1 for electrons and $+1$ for protons, the double-ionization cross sections can be expressed as

$$\sigma^{2+} = a(v_p) \pm b(v_p) + c(v_p) ,$$

where a, b, and c are positive and depend on the projectile velocity. The plus sign holds for electron bombardment and the minus sign for proton bombardment. The

ratio of the electron-induced to the proton-induced cross section can be written

$$\frac{\sigma^{2+}(e^-)}{\sigma^{2+}(p^+)} = \frac{a+b+c}{a-b+c} .$$

It is approximately constant for the projectile energy range of 750 keV/amu to the experimental limit of 3500 keV/amu. The total double-ionization cross sections for both electron and proton bombardment decrease with increasing energy, but the constant value of the ratio indicates that the interference term is remaining a fixed fraction of the sum of the first and second Born terms, i.e., $b = k(a+c)$.

B. Ionization plus excitation

The cross sections for ionization plus excitation to all of the states considered, viz., the $2p\sigma_u$, $2p\pi_u$, and $2s\sigma_g$ states, by electrons and protons are shown in Fig. 9 and listed separately in Table II. Just as seen in double ionization, the ratio of these cross sections is approximately 2. However, for ionization plus excitation, the ratio peaks at about 1000–1500 keV/amu and then decreases. The ratios for each state separately show this same behavior.

If the ionization plus excitation cross section is expressed in a Born series, as was done for double ionization, then

$$(\sigma^+)^* = d(v_p) \pm e(v_p) + f(v_p) ,$$

where d, e, and f are positive and depend on the projectile velocity. As before, the plus sign holds for electrons

TABLE I. Double-ionization cross sections of H_2 by electrons and protons oriented at 90° relative to the projectile direction.

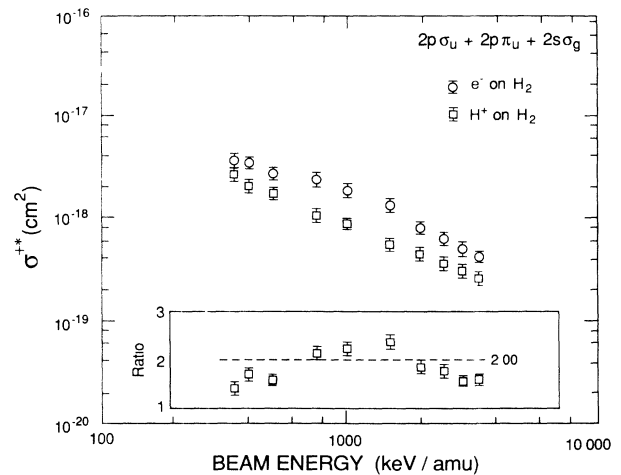| Projectile	$(\sigma^2)^+$ $(10^{-20}$ cm$^2)$	
keV/amu	Electrons	Protons
350	43.0±6.5	41.1±6.2
400	41.6±6.2	34.4±5.2
500	29.2±4.4	23.9±3.6
750	26.1±3.9	13.2±2.0
1000	19.3±2.9	8.82±1.32
1500	15.2±2.3	5.63±0.84
2000	9.49±1.42	4.44±0.67
2500	8.06±1.21	3.49±0.52
3000	6.58±0.99	2.69±0.40
3500	5.77±0.87	2.28±0.34

FIG. 9. Cross sections for ionization plus excitation of H_2 by electrons and protons. Ratios of cross sections by electrons to protons are shown in the enclosed box.

TABLE II. Ionization plus excitation cross sections of the H_2 by electrons and protons oriented at 90° relative to the projectile direction.

Projectile (keV/amu)	$(\sigma^+)^*(10^{-20}\ cm^2)\pm15\%$					
	Electrons			Protons		
	$2s\sigma_g$	$2p\sigma_u$	$2p\pi_u$	$2s\sigma_g$	$2p\sigma_u$	$2p\pi_u$
350	103	203	85.4	56.6	143	68.9
400	97.8	188	80.0	51.2	111	49.5
500	68.8	149	60.5	40.9	91.3	40.8
750	66.4	129	44.6	27.5	59.1	24.7
1000	49.4	104	39.8	20.2	45.8	20.2
1500	40.4	75.3	26.7	15.2	31.3	12.4
2000	22.2	46.9	15.9	12.1	24.8	9.31
2500	17.8	36.9	11.5	11.1	20.2	6.33
3000	14.6	28.7	8.60	8.48	18.3	6.33
3500	12.5	23.7	7.11	7.04	15.2	4.82

and the minus sign for protons. The ratio

$$\frac{(\sigma^+)^*(e^-)}{(\sigma^+)^*(p^+)} = \frac{d+e+f}{d-e+f}$$

is a decreasing function as the projectile energy increases above 1500 keV/amu. This suggests that the interference contribution is decreasing relative to the first and second Born parts.

C. Double excitation

As described above, the doubly excited states of H_2 cannot be resolved in our experiment. The cross sections for excitation to the modeled channel by electrons and protons are shown in Fig. 10. Once again, the electron cross sections are greater than the proton cross sections. This is in contrast to the results for excitation of doubly excited states of helium[5] where no difference is seen for excitation of the unresolved $2p^2\ {}^1D$ and $2s2p\ {}^1P^o$ states. The present results do not permit detailed analysis since we cannot be at all sure of the relative contribution of the

three autoionizing states under consideration. The best results of the fitting routine were obtained with a mixture of $\sigma_u^2\ {}^1\Sigma_g^+$ and $\sigma_u\pi_u\ {}^1\Pi_g$ states shown in Fig. 6. We experimented with a wide variety of mixtures in order to determine the effect of the choice on the results of the fitting procedure. We found that only the value of the cross section for the $2p\pi_u$ channel was significantly affected. The absolute cross section varied by as much as 20%, but the relative cross section did not change in energy dependence.

V. DISCUSSION

A. Comparison of $(\sigma^+)^*$ to $(\sigma^2)^+$

The ratios of the cross sections for ionization plus excitation to double ionization are shown in Fig. 11 for both
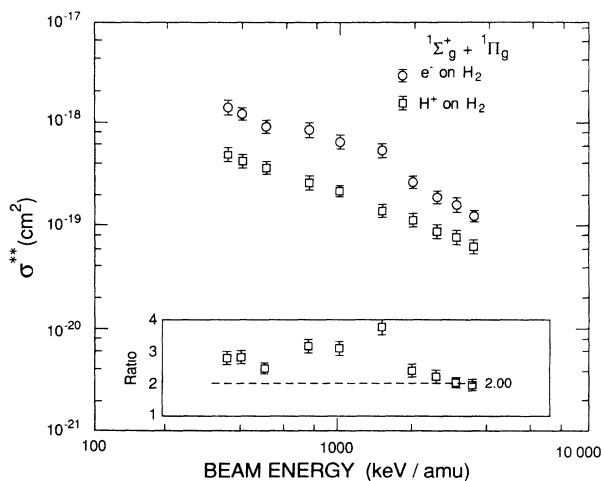

FIG. 10. Cross sections for double excitation of H_2 by electrons and protons. Ratios of cross sections by electrons to protons are shown in the enclosed box.
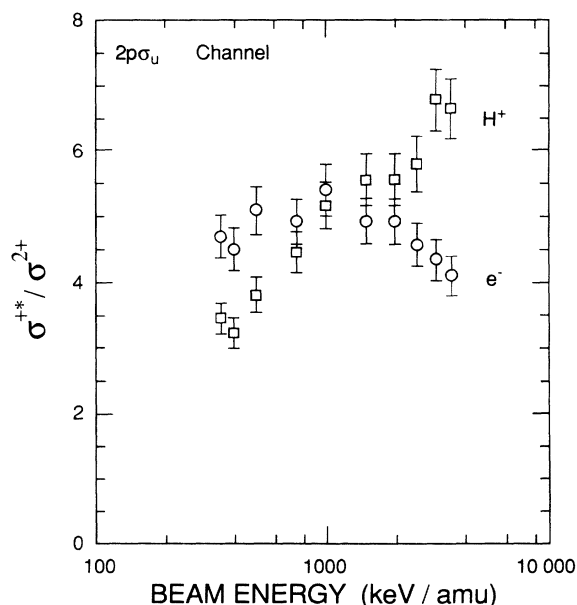

FIG. 11. Ratios of cross sections for ionization plus excitation to double ionization for electron and proton collisions for the $2p\sigma_u$ channel.
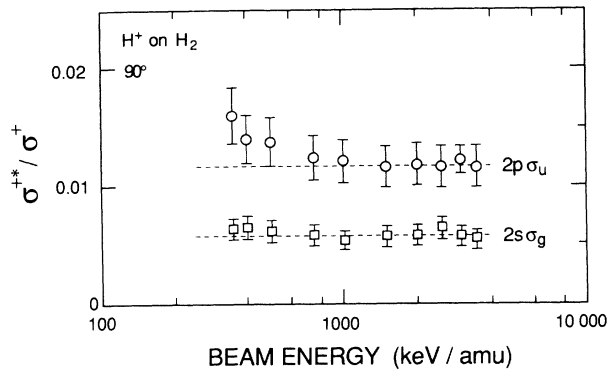
FIG. 12. Ratios of cross sections for ionization plus excitation to single ionization for proton collisions for the $2p\sigma_u$ and $2s\sigma_g$ channels.

electron and proton bombardment for the $2p\sigma_u$ channel. The other channels show similar behavior. If these ratios are expressed in a Born series, then, for electron projectiles,

$$\frac{(\sigma^+)^*}{(\sigma^2)^+} = \frac{d+e+f}{a+b+c} ,$$

and for proton projectiles

$$\frac{(\sigma^+)^*}{(\sigma^2)^+} = \frac{d-e+f}{a-b+c} .$$

The electron data fall off at higher energies while the proton data rise. This behavior can occur if the interference term for ionization plus excitation, $e(v_p)$ falls off faster with projectile velocity than does the interference term for double ionization $b(v_p)$ relative to the first and second Born parts. This supports the same conclusion that was drawn in Sec. IV.

B. Comparison of $(\sigma^+)^*$ to σ^+

1. Low-velocity collisions

The ratios of cross sections for ionization plus excitation to single ionization for proton bombardment are shown in Fig. 12 for the $2p\sigma_u$ and $2s\sigma_g$ channels. The $2p\sigma_u$ data (and the $2p\pi_u$ data which are not included in the figure) show a rise at low energy which is believed to arise from a large second Born contribution that consists of two dipole excitations in the double-collision process. The $2s\sigma_g$ data do not have this rise and the second Born contribution to the data consists of either a dipole and a nondipole transition or two nondipole transitions. The electron data at low velocities are strongly influenced by the ionization plus excitation threshold, so a plot similar to Fig. 12 cannot be discussed in the same terms. The single-ionization cross sections used in calculating the ratios are the preferred values of Rudd et al.[42] for electron production.
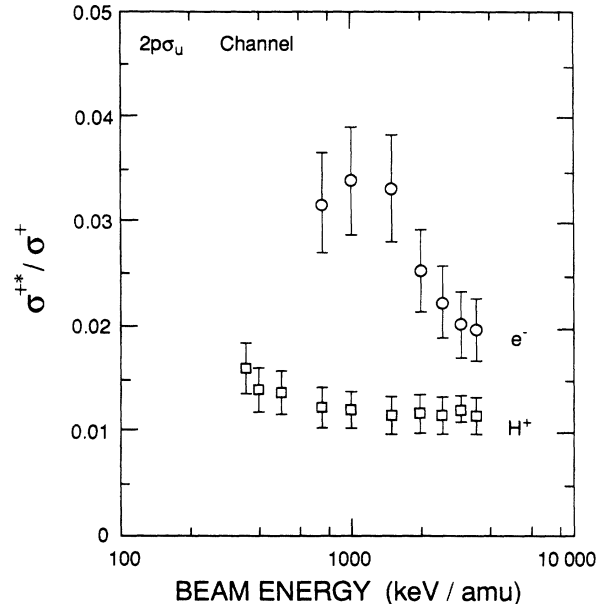

FIG. 13. Ratios of cross sections for ionization plus excitation to single ionization for proton and electron collisions for the $2p\sigma_u$ channel.

2. High-energy collisions

The ratios of cross sections for ionization plus excitation to single ionization for proton and electron bombardment are shown in Fig. 13 for the $2p\sigma_u$ channel. At high velocities, away from the threshold for electron bombardment, the Born series for $(\sigma^+)^*$ has been expressed above as

$$(\sigma^+)^* = d \pm e + f .$$

If e and f are of about the same magnitude (as was found for double ionization of helium studied by Reading and Ford[12]) then $(\sigma^+)^* \sim d$ for protons and $(\sigma^+)^* = d + e + f$ for electrons. The ratio $(\sigma^+)^*/\sigma^+$ for proton collisions is a ratio of first Born terms (this assumes that σ^+ is mostly first Born), and it is constant as a function of collision velocity. The ratio $(\sigma^+)^*/\sigma^+$ for electron collisions has contributions from the interference and second Born terms of $(\sigma^+)^*$ and therefore decreases with collision velocity. The single-ionization cross sections used in calculating the ratios for electron collisions are those of Edwards et al.[21]

ACKNOWLEDGMENTS

[1]S. L. Carter and H. P. Kelly, Phys. Rev. A **16**, 1525 (1977).

[2]L. H. Andersen, P. Hvelplund, H. Knudsen, S. P. Møller, A. H. Sorensen, K. Elsener, K.-G. Rensfelt, and E. Uggerhøj, Phys. Rev. A **36**, 3612 (1987).

[3]L. H. Andersen, P. Hvelplund, H. Knudsen, S. P. Møller, K. Elsener, K.-G. Rensfelt, and E. Uggerhøj, Phys. Rev. Lett. **57**, 2147 (1986).

[4]M. Charlton, L. H. Andersen, L. Brun-Nielsen, B. I. Deutch, P. Hvelplund, F. M. Jacobsen, H. Knudsen, G. Laricchia, M. R. Poulsen, and J. O. Pedersen, J. Phys. B **21**, L545 (1988).

[5]J. O. P. Pedersen and P. Hvelplund, Phys. Rev. Lett. **62**, 2373 (1989).

[6]H. Knudsen, L. H. Andersen, P. Hvelplund, J. Sørensen, and C. Ciric, J. Phys. B **20**, L253 (1987).

[7]M. B. Shah and H. B. Gilbody, J. Phys. B **18**, 899 (1985).

[8]R. D. DuBois, L. H. Toburen, and M. E. Rudd, Phys. Rev. A **29**, 70 (1984).

[9]R. D. DuBois and L. H. Toburen, Phys. Rev. A **38**, 3960 (1988).

[10]E. Y. Kamber, C. L. Cocke, S. Cheng, and S. L. Varghese, Phys. Rev. Lett. **60**, 2026 (1988).

[11]R. M. Wood, A. K. Edwards, and R. L. Ezell, Phys. Rev. A **34**, 4415 (1986).

[12]J. F. Reading and A. L. Ford, J. Phys. B **20**, 3747 (1987).

[13]J. H. McGuire, Phys. Rev. Lett. **49**, 1153 (1982).

[14]J. H. McGuire, Phys. Rev. A **36**, 1114 (1987).

[15]L. Vegh, Phys. Rev. A **37**, 992 (1988).

[16]R. E. Olson, Phys. Rev. A **36**, 1519 (1987).

[17]A. L. Ford and J. F. Reading, Nucl. Instrum. Methods B **40/41**, 362 (1989).

[18]T. Watanake and L. Végh, Nucl. Instrum. Methods B **40/41**, 89 (1989).

[19]J. F. Reading and A. L. Ford, Phys. Rev. Lett. **58**, 543 (1987).

[20]A. L. Ford and J. F. Reading, J. Phys. B **21**, L685 (1988).

[21]A. K. Edwards, R. M. Wood, A. S. Beard, and R. L. Ezell, Phys. Rev. A **37**, 3697 (1988).

[22]A. K. Edwards, R. M. Wood, and R. L. Ezell, Phys. Rev. A **34**, 4411 (1986).

[23]D. R. Bates, K. Ledsham, and A. L. Stewart, Philos. Trans. Soc. London Ser. A **246**, 215 (1953).

[24]T. E. Sharp, At. Data **2**, 119 (1971).

[25]G. Herzberg, *Electronic Spectra of Polyatomic Molecules* (Van Nostrand Reinhold, New York, 1966), Appendix IV.

[26]R. M. Wood, A. K. Edwards, and M. F. Steuer, Rev. Sci. Instrum. **47**, 1471 (1976).

[27]R. M. Wood, A. K. Edwards, and M. F. Steuer, Phys. Rev. A **15**, 1433 (1977).

[28]A. K. Edwards, R. M. Wood, and R. L. Ezell, Phys. Rev. A **31**, 99 (1985).

[29]P. H. Doolittle, R. J. Schoen, and K. E. Schubert, J. Chem. Phys. **49**, 5108 (1968).

[30]M. F. Steuer, R. M. Wood, and A. K. Edwards, Phys. Rev. A **16**, 1873 (1977).

[31]A. K. Edwards and R. M. Wood, J. Chem. Phys. **76**, 2938 (1982).

[32]R. M. Wood, A. K. Edwards, and R. L. Ezell, Radiat. Phys. Chem. **26**, 635 (1985).

[33]Alain Huetz (private communication).

[34]A. K. Edwards, R. M. Wood, and M. F. Steuer, Phys. Rev. A **16**, 1385 (1977).

[35]T. G. Heil (private communication).

[36]R. N. Zare and J. K. Cashion, Lawrence Berkeley Laboratory Report No. UCRL-10881, 1963.

[37]R. A. Buckingham, in *Quantum Theory I, Elements,* edited by D. R. Bates (Academic, New York, 1961).

[38]M. Misakian and J. C. Zorn, Phys. Rev. A **6**, 2180 (1972).

[39]S. L. Guberman, J. Chem. Phys. **78**, 1404 (1983).

[40]J. Tennyson and C. J. Noble, J. Phys. B **18**, 155 (1985).

[41]H. Kossmann, O. Schwarzkopf, and V. Schmidt (unpublished).

[42]M. E. Rudd, Y.-K. Kim, D. H. Madison, and J. W. Gallagher, Rev. Mod. Phys. **57**, 965 (1985).